

Topological insulators in Bi_2Se_3 , Bi_2Te_3 and Sb_2Te_3 with a single Dirac cone on the surface

Haijun Zhang¹, Chao-Xing Liu², Xiao-Liang Qi³, Xi Dai¹, Zhong Fang¹ and Shou-Cheng Zhang^{3*}

Topological insulators are new states of quantum matter in which surface states residing in the bulk insulating gap of such systems are protected by time-reversal symmetry. The study of such states was originally inspired by the robustness to scattering of conducting edge states in quantum Hall systems. Recently, such analogies have resulted in the discovery of topologically protected states in two-dimensional and three-dimensional band insulators with large spin-orbit coupling. So far, the only known three-dimensional topological insulator is $\text{Bi}_x\text{Sb}_{1-x}$, which is an alloy with complex surface states. Here, we present the results of first-principles electronic structure calculations of the layered, stoichiometric crystals Sb_2Te_3 , Sb_2Se_3 , Bi_2Te_3 and Bi_2Se_3 . Our calculations predict that Sb_2Te_3 , Bi_2Te_3 and Bi_2Se_3 are topological insulators, whereas Sb_2Se_3 is not. These topological insulators have robust and simple surface states consisting of a single Dirac cone at the Γ point. In addition, we predict that Bi_2Se_3 has a topologically non-trivial energy gap of 0.3 eV, which is larger than the energy scale of room temperature. We further present a simple and unified continuum model that captures the salient topological features of this class of materials.

Recently, the subject of time-reversal-invariant topological insulators has attracted great attention in condensed-matter physics^{1–12}. Topological insulators in two or three dimensions have insulating energy gaps in the bulk, and gapless edge or surface states on the sample boundary that are protected by time-reversal symmetry. The surface states of a three-dimensional (3D) topological insulator consist of an odd number of massless Dirac cones, with a single Dirac cone being the simplest case. The existence of an odd number of massless Dirac cones on the surface is ensured by the Z_2 topological invariant^{7–9} of the bulk. Furthermore, owing to the Kramers theorem, no time-reversal-invariant perturbation can open up an insulating gap at the Dirac point on the surface. However, a topological insulator can become fully insulating both in the bulk and on the surface if a time-reversal-breaking perturbation is introduced on the surface. In this case, the electromagnetic response of three-dimensional (3D) topological insulators is described by the topological θ term of the form $S_\theta = (\theta/2\pi)(\alpha/2\pi) \int d^3x dt \mathbf{E} \cdot \mathbf{B}$, where \mathbf{E} and \mathbf{B} are the conventional electromagnetic fields and α is the fine-structure constant¹⁰. $\theta = 0$ describes a conventional insulator, whereas $\theta = \pi$ describes topological insulators. Such a physically measurable and topologically non-trivial response originates from the odd number of Dirac fermions on the surface of a topological insulator.

Soon after the theoretical prediction⁵, the 2D topological insulator exhibiting the quantum spin Hall effect was experimentally observed in HgTe quantum wells⁶. The electronic states of the 2D HgTe quantum wells are well described by a 2 + 1-dimensional Dirac equation where the mass term is continuously tunable by the thickness of the quantum well. Beyond a critical thickness, the Dirac mass term of the 2D quantum well changes sign from being positive to negative, and a pair of gapless helical edge states appears inside the bulk energy gap. This microscopic mechanism for obtaining topological insulators by inverting the bulk Dirac gap spectrum can also be generalized to other 2D and 3D systems. The guiding principle is to search for insulators where the

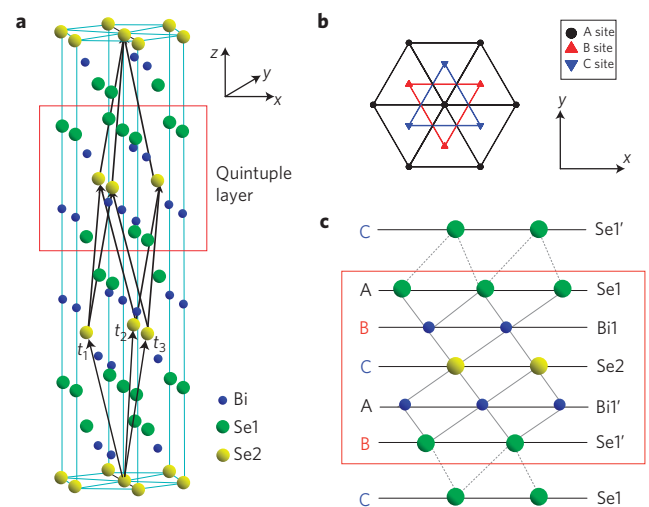


Figure 1 | Crystal structure. **a**, Crystal structure of Bi_2Se_3 with three primitive lattice vectors denoted as $\mathbf{t}_{1,2,3}$. A quintuple layer with $\text{Se1-Bi1-Se2-Bi1'-Se1'}$ is indicated by the red square. **b**, Top view along the z -direction. The triangle lattice in one quintuple layer has three different positions, denoted as A, B and C. **c**, Side view of the quintuple layer structure. Along the z -direction, the stacking order of Se and Bi atomic layers is $\dots\text{-C(Se1')-A(Se1)-B(Bi1)-C(Se2)-A(Bi1')-B(Se1')-C(Se1)-\dots$. The Se1 (Bi1) layer can be related to the Se1' (Bi1') layer by an inversion operation in which the Se2 atoms have the role of inversion centres.

conduction and the valence bands have the opposite parity, and a 'band inversion' occurs when the strength of some parameter, say the spin-orbit coupling (SOC), is tuned. For systems with inversion symmetry, a method based on the parity eigenvalues of band states at time-reversal-invariant points can be applied¹³. On the basis of this analysis, the $\text{Bi}_x\text{Sb}_{1-x}$ alloy has been predicted

¹Beijing National Laboratory for Condensed Matter Physics, and Institute of Physics, Chinese Academy of Sciences, Beijing 100190, China, ²Center for Advanced Study, Tsinghua University, Beijing 100084, China, ³Department of Physics, McCullough Building, Stanford University, Stanford, California 94305-4045, USA. *e-mail: sczhang@stanford.edu.

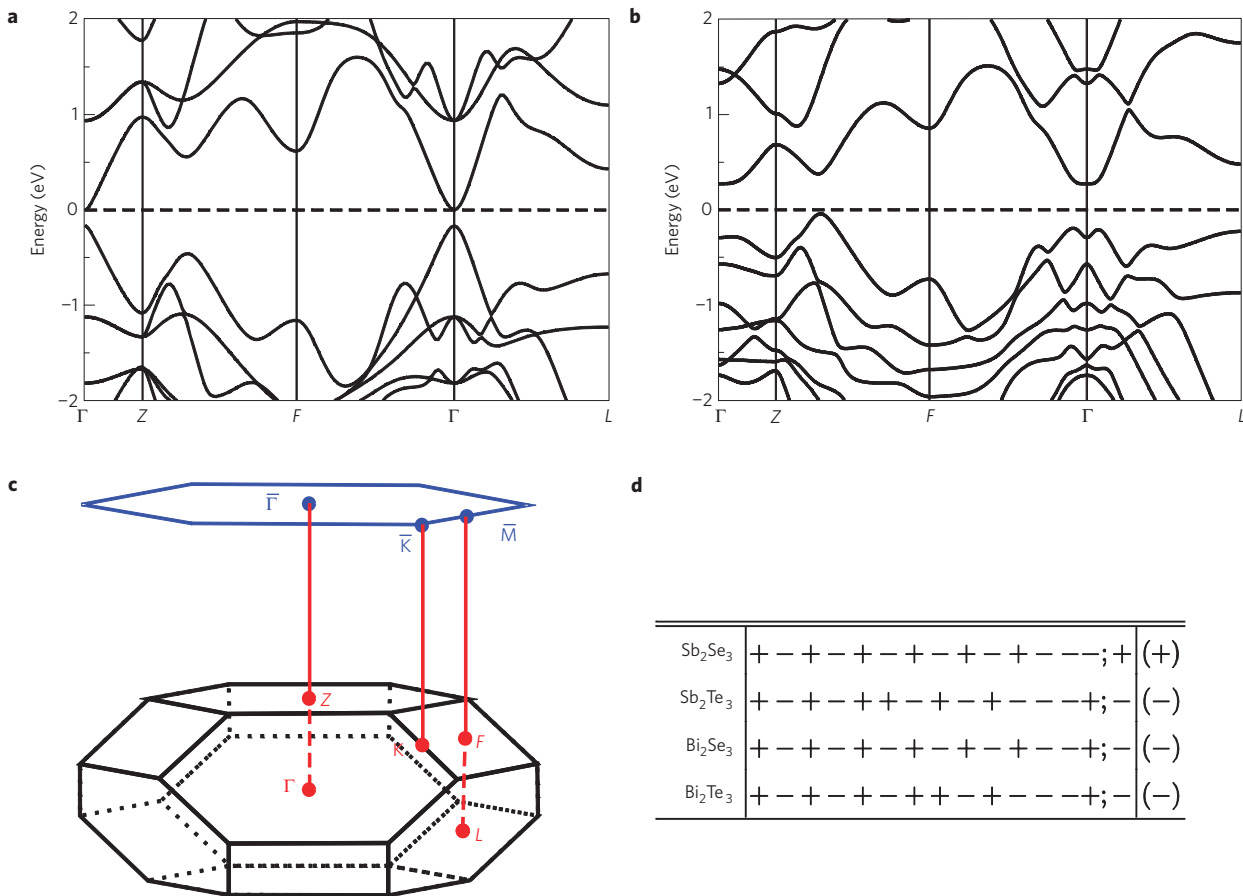


Figure 2 | Band structure, Brillouin zone and parity eigenvalues. **a, b**, Band structure for Bi_2Se_3 without **(a)** and with **(b)** SOC. The dashed line indicates the Fermi level. **c**, Brillouin zone for Bi_2Se_3 with space group $R\bar{3}m$. The four inequivalent time-reversal-invariant points are $\Gamma(0, 0, 0)$, $L(\pi, 0, 0)$, $F(\pi, \pi, 0)$ and $Z(\pi, \pi, \pi)$. The blue hexagon shows the 2D Brillouin zone of the projected $(1, 1, 1)$ surface, in which the high-symmetry \mathbf{k} points $\bar{\Gamma}$, \bar{K} and \bar{M} are labelled. **d**, The parity of the band at the Γ point for the four materials Sb_2Te_3 , Sb_2Se_3 , Bi_2Se_3 and Bi_2Te_3 . Here, we show the parities of fourteen occupied bands, including five s bands and nine p bands, and the lowest unoccupied band. The product of the parities for the fourteen occupied bands is given in brackets on the right of each row.

to be a topological insulator for a small range of x , and recently, surface states with an odd number of crossings at the Fermi energy have been observed in angle-resolved photoemission spectroscopy (ARPES) experiments¹².

As $\text{Bi}_x\text{Sb}_{1-x}$ is an alloy with random substitutional disorder, its electronic structures and dispersion relations are only defined within the mean field, or the coherent potential approximation. Its surface states are also extremely complex, with as many as five or possibly more dispersion branches, which are not easily describable by simple theoretical models. Alloys also tend to have impurity bands inside the nominal bulk energy gap, which could overlap with the surface states. Given the importance of topological insulators as new states of quantum matter, it is important to search for material systems that are stoichiometric crystals with well-defined electronic structures, preferably with simple surface states, and describable by simple theoretical models. Here, we focus on layered, stoichiometric crystals Sb_2Te_3 , Sb_2Se_3 , Bi_2Te_3 and Bi_2Se_3 . Our theoretical calculations predict that Sb_2Te_3 , Bi_2Te_3 and Bi_2Se_3 are topological insulators, whereas Sb_2Se_3 is not. Most importantly, our theory predicts that Bi_2Se_3 has a topologically non-trivial energy gap of 0.3 eV, larger than the energy scale of room temperature. The topological surface states for these crystals are extremely simple, described by a single gapless Dirac cone at the $\mathbf{k} = 0$ Γ point in the surface Brillouin zone. We also propose a simple and unified continuum model that captures the salient topological features of this class of materials. In this

precise sense, this class of 3D topological insulators shares the great simplicity of the 2D topological insulators realized in the HgTe quantum wells.

Band structure and parity analysis

Bi_2Se_3 , Bi_2Te_3 , Sb_2Te_3 and Sb_2Se_3 share the same rhombohedral crystal structure with the space group D_{3d}^5 ($R\bar{3}m$) with five atoms in one unit cell. We take Bi_2Se_3 as an example and show its crystal structure in Fig. 1a, which has layered structures with a triangle lattice within one layer. It has a trigonal axis (three-fold rotation symmetry), defined as the z axis, a binary axis (two-fold rotation symmetry), defined as the x axis, and a bisectrix axis (in the reflection plane), defined as the y axis. The material consists of five-atom layers arranged along the z -direction, known as quintuple layers. Each quintuple layer consists of five atoms with two equivalent Se atoms (denoted as Se1 and Se1' in Fig. 1c), two equivalent Bi atoms (denoted as Bi1 and Bi1' in Fig. 1c) and a third Se atom (denoted as Se2 in Fig. 1c). The coupling is strong between two atomic layers within one quintuple layer but much weaker, predominantly of the van der Waals type, between two quintuple layers. The primitive lattice vectors $\mathbf{t}_{1,2,3}$ and rhombohedral unit cells are shown in Fig. 1a. The Se2 site has the role of an inversion centre and under an inversion operation, Bi1 is changed to Bi1' and Se1 is changed to Se1'. The existence of inversion symmetry enables us to construct eigenstates with definite parity for this system.

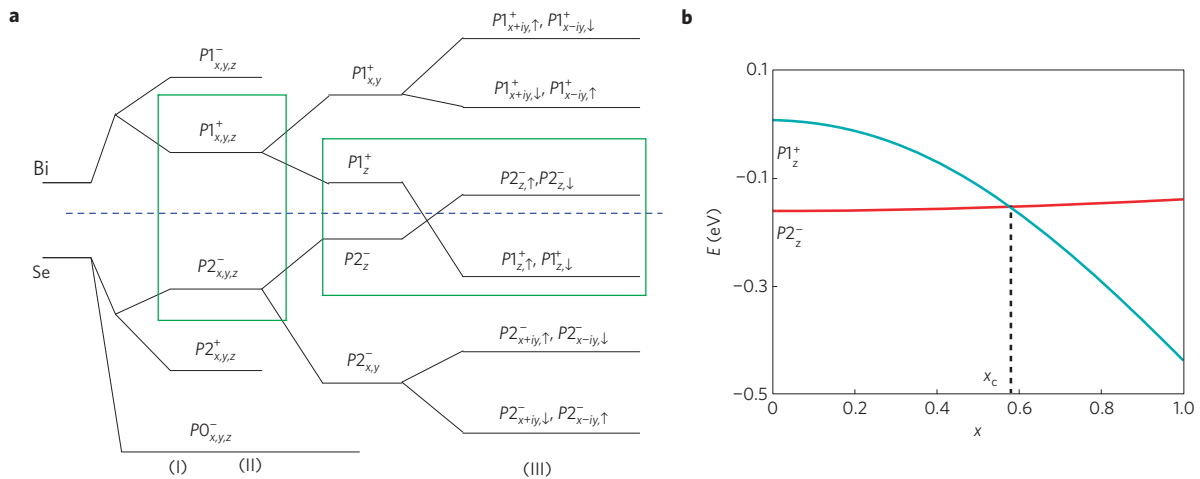


Figure 3 | Band sequence. **a**, Schematic diagram of the evolution from the atomic $p_{x,y,z}$ orbitals of Bi and Se into the conduction and valence bands of Bi_2Se_3 at the Γ point. The three different stages (I), (II) and (III) represent the effect of turning on chemical bonding, crystal-field splitting and SOC, respectively (see text). The blue dashed line represents the Fermi energy. **b**, The energy levels $|P1_z^+\rangle$ and $|P2_z^-\rangle$ of Bi_2Se_3 at the Γ point versus an artificially rescaled atomic SOC $\lambda(\text{Bi}) = x\lambda_0(\text{Bi}) = 1.25x$ eV, $\lambda(\text{Se}) = x\lambda_0(\text{Se}) = 0.22x$ eV (see text). A level crossing occurs between these two states at $x = x_c \approx 0.6$.

Ab initio calculations for Sb_2Te_3 , Sb_2Se_3 , Bi_2Te_3 and Bi_2Se_3 are carried out in the framework of the Perdew–Burke–Ernzerhof-type¹⁴ generalized gradient approximation of the density functional theory. The BSTATE package¹⁵ with the plane-wave pseudopotential method is used with a \mathbf{k} -point grid taken as $10 \times 10 \times 10$ and the kinetic energy cutoff fixed to 340 eV. For Sb_2Te_3 , Bi_2Te_3 and Bi_2Se_3 , the lattice constants are chosen from experiments, whereas for Sb_2Se_3 , the lattice parameters are optimized in the self-consistent calculation for rhombohedral crystal structure ($a = 4.076$ Å, $c = 29.830$ Å), owing to the lack of experimental data.

Our results are consistent with the previous calculations^{16,17}. In particular, we note that Bi_2Se_3 has an energy gap of about 0.3 eV, which agrees well with the experimental data (about 0.2–0.3 eV; refs 18, 19). In the following, we take the band structure of Bi_2Se_3 as an example. Figure 2a and b show the band structure of Bi_2Se_3 without and with SOC, respectively. By comparing the two figure parts, one can see clearly that the only qualitative change induced by turning on SOC is an anti-crossing feature around the Γ point, which thus indicates an inversion between the conduction band and valence band due to SOC effects, suggesting that Bi_2Se_3 is a topological insulator. To firmly establish the topological nature of this material, we follow the method proposed by Fu and Kane¹³. Thus, we calculate the product of the parities of the Bloch wavefunction for the occupied bands at all time-reversal-invariant momenta Γ, F, L, Z in the Brillouin zone. As expected, we find that at the Γ point, the parity of one occupied band is changed on turning on SOC, whereas the parity remains unchanged for all occupied bands at the other momenta F, L, Z . As the system without SOC is guaranteed to be a trivial insulator, we conclude that Bi_2Se_3 is a strong topological insulator. The same calculation is carried out for the other three materials, from which we find that Sb_2Te_3 and Bi_2Te_3 are also strong topological insulators, and Sb_2Se_3 is a trivial insulator. The parity eigenvalues of the highest 14 bands below the Fermi level and the first conduction band at the Γ point are listed in Fig. 2d. From this table we can see that the product of parities of occupied bands at the Γ point changes from the trivial material Sb_2Se_3 to the three non-trivial materials, owing to an exchange of the highest occupied state and the lowest unoccupied state. This agrees with our earlier analysis that an inversion between the conduction band and valence band occurs at the Γ point.

To get a better understanding of the inversion and the parity exchange, we start from the atomic energy levels and consider the effect of crystal-field splitting and SOC on the energy eigenvalues

at the Γ point. This is summarized schematically in three stages (I), (II) and (III) in Fig. 3a. As the states near the Fermi surface are mainly coming from p orbitals, we will neglect the effect of s orbitals and start from the atomic p orbitals of Bi ($6s^26p^3$) and Se ($4s^24p^4$). In stage (I), we consider the chemical bonding between Bi and Se atoms within a quintuple layer, which is the largest energy scale in the current problem. First we can recombine the orbitals in a single unit cell according to their parity, which results in three states (two odd, one even) from each Se p orbital and two states (one odd, one even) from each Bi p orbital. The formation of chemical bonding hybridizes the states on Bi and Se atoms, thus pushing down all of the Se states and lifting up all of the Bi states. In Fig. 3a, these five hybridized states are labelled as $|P1_{x,y,z}^\pm\rangle$, $|P2_{x,y,z}^\pm\rangle$ and $|P0_{x,y,z}^-\rangle$, where the superscripts $+$, $-$ stand for the parity of the corresponding states. In stage (II), we consider the effect of the crystal-field splitting between different p orbitals. According to the point-group symmetry, the p_z orbital is split from the p_x and p_y orbitals whereas the last two remain degenerate. After this splitting, the energy levels closest to the Fermi energy turn out to be the p_z levels $|P1_z^+\rangle$ and $|P2_z^-\rangle$. In the last stage (III), we take into account the effect of SOC. The atomic SOC Hamiltonian is given by $H_{\text{so}} = \lambda \mathbf{l} \cdot \mathbf{S}$, with \mathbf{l}, \mathbf{S} being the orbital and spin angular momentum, and λ is the SOC parameter. The SOC Hamiltonian mixes spin and orbital angular momenta while preserving the total angular momentum, which thus leads to a level repulsion between $|P1_z^+, \uparrow\rangle$ and $|P1_{x+iy}^+, \downarrow\rangle$, and similar combinations. Consequently, the $|P1_z^+, \uparrow(\downarrow)\rangle$ state is pushed down by the SOC effect and the $|P2_z^-, \uparrow(\downarrow)\rangle$ state is pushed up. If the SOC is large enough ($\lambda > \lambda_c$), the order of these two levels is reversed. To see this inversion process explicitly, we also calculate the energy levels $|P1_z^+\rangle$ and $|P2_z^-\rangle$ for a model Hamiltonian of Bi_2Se_3 with artificially rescaled atomic SOC parameters $\lambda(\text{Bi}) = x\lambda_0(\text{Bi})$, $\lambda(\text{Se}) = x\lambda_0(\text{Se})$, as shown in Fig. 3b. Here, $\lambda_0(\text{Bi}) = 1.25$ eV and $\lambda_0(\text{Se}) = 0.22$ eV are the realistic values of Bi and Se atomic SOC parameters, respectively²⁰. From Fig. 3b, one can see clearly that a level crossing occurs between $|P1_z^+\rangle$ and $|P2_z^-\rangle$ when the SOC is about 60% of the realistic value. As these two levels have opposite parity, the inversion between them drives the system into a topological insulator phase. Therefore, the mechanism for the 3D topological insulator in this system is exactly analogous to the mechanism in the 2D topological insulator HgTe. In summary, through the analysis above we find that Bi_2Se_3 is topologically non-trivial due to the inversion between two p_z orbitals with opposite parity at the Γ point. Similar analyses can

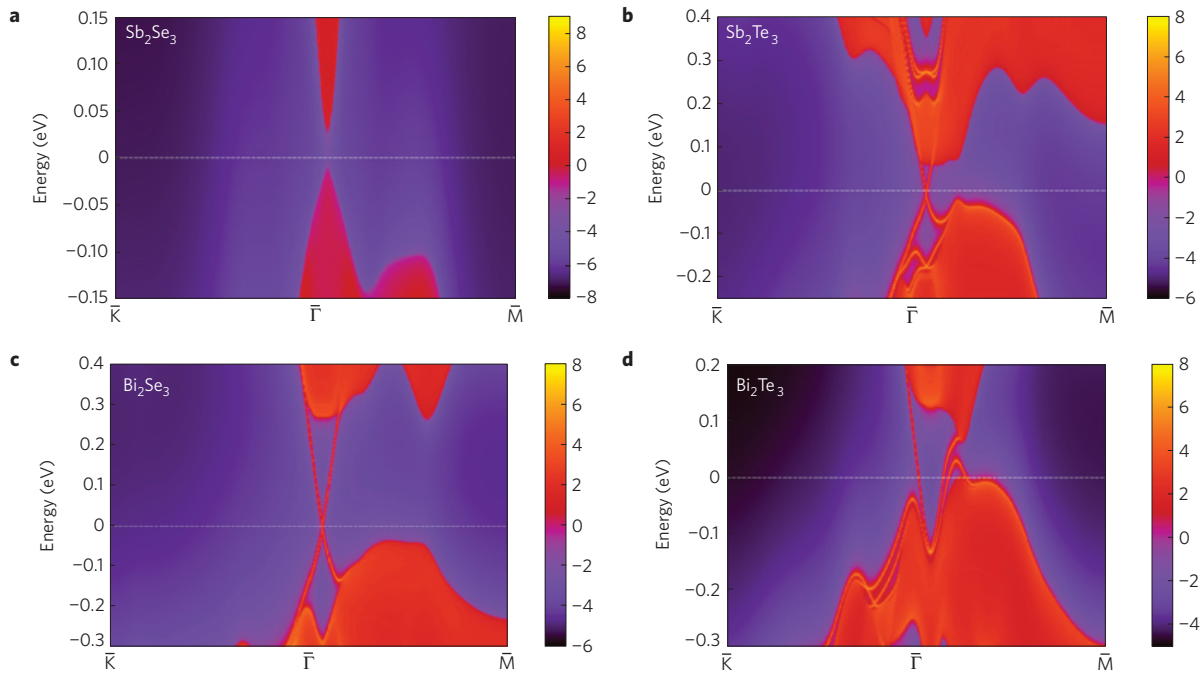


Figure 4 | Surface states. **a–d**, Energy and momentum dependence of the LDOS for Sb_2Se_3 (**a**), Sb_2Te_3 (**b**), Bi_2Se_3 (**c**) and Bi_2Te_3 (**d**) on the [111] surface. Here, the warmer colours represent higher LDOS. The red regions indicate bulk energy bands and the blue regions indicate bulk energy gaps. The surface states can be clearly seen around the Γ point as red lines dispersing in the bulk gap for Sb_2Te_3 , Bi_2Se_3 and Bi_2Te_3 . No surface state exists for Sb_2Se_3 .

be carried out on the other three materials, from which we see that Sb_2Te_3 and Bi_2Te_3 are qualitatively the same as Bi_2Se_3 , whereas the SOC of Sb_2Te_3 is not strong enough to induce such an inversion.

Topological surface states

The existence of topological surface states is one of the most important properties of the topological insulators. To see the topological features of the four systems explicitly, we calculate the surface states of these four systems on the basis of an *ab initio* calculation. First we construct the maximally localized Wannier function (MLWF) from the *ab initio* calculation using the method developed by Marzari and co-workers^{21,22}. We divide the semi-infinite system into a surface slab with finite thickness and the remaining part as the bulk. The MLWF hopping parameters for the bulk part can be constructed from the bulk *ab initio* calculation, and the ones for the surface slab can be constructed from the *ab initio* calculation of the slab, in which the surface correction to the lattice constants and band structure have been considered self-consistently and the chemical potential is determined by the charge neutrality condition. With these bulk and surface MLWF hopping parameters, we use an iterative method^{23,24} to obtain the surface Green's function of the semi-infinite system. The imaginary part of the surface Green's function is the local density of states (LDOS), from which we can obtain the dispersion of the surface states. The surface LDOS on the [111] surface for all four systems is shown in Fig. 4. For Sb_2Te_3 , Bi_2Se_3 and Bi_2Te_3 , one can clearly see the topological surface states that form a single Dirac cone at the Γ point. In comparison, Sb_2Se_3 has no surface state and is a topologically trivial insulator. Thus, the surface-state calculation agrees well with the bulk parity analysis, and confirms conclusively the topologically non-trivial nature of the three materials. For Bi_2Se_3 , the Fermi velocity of the topological surface states is $v_F \simeq 5.0 \times 10^5 \text{ m s}^{-1}$, which is similar to that of the other two materials.

Low-energy effective model

As the topological nature is determined by the physics near the Γ point, it is possible to write down a simple effective Hamiltonian

to characterize the low-energy long-wavelength properties of the system. Starting from the four low-lying states $|P1_z^+, \uparrow (\downarrow)\rangle$ and $|P2_z^-, \uparrow (\downarrow)\rangle$ at the Γ point, such a Hamiltonian can be constructed by the theory of invariants²⁵ for the finite wave vector \mathbf{k} . On the basis of the symmetries of the system, the generic form of the 4×4 effective Hamiltonian can be written down up to the order of $O(\mathbf{k}^2)$, and the tunable parameters in the Hamiltonian can be obtained by fitting the band structure of our *ab initio* calculation. The important symmetries of the system are time-reversal symmetry T , inversion symmetry I and three-fold rotation symmetry C_3 along the z axis. In the basis of $(|P1_z^+, \uparrow\rangle, |P2_z^-, \uparrow\rangle, |P1_z^+, \downarrow\rangle, |P2_z^-, \downarrow\rangle)$, the representation of the symmetry operations is given by $T = \mathcal{K} \cdot i\sigma^y \otimes I_{2 \times 2}$, $I = I_{2 \times 2} \otimes \tau_3$ and $C_3 = \exp(i(\pi/3)\sigma^z \otimes I_{2 \times 2})$, where \mathcal{K} is the complex conjugation operator, $\sigma^{x,y,z}$ and $\tau^{x,y,z}$ denote the Pauli matrices in the spin and orbital space, respectively. By requiring these three symmetries and keeping only the terms up to quadratic order in \mathbf{k} , we obtain the following generic form of the effective Hamiltonian:

$$H(\mathbf{k}) = \epsilon_0(\mathbf{k})I_{4 \times 4} + \begin{pmatrix} \mathcal{M}(\mathbf{k}) & A_1 k_z & 0 & A_2 k_- \\ A_1 k_z & -\mathcal{M}(\mathbf{k}) & A_2 k_- & 0 \\ 0 & A_2 k_+ & \mathcal{M}(\mathbf{k}) & -A_1 k_z \\ A_2 k_+ & 0 & -A_1 k_z & -\mathcal{M}(\mathbf{k}) \end{pmatrix} + o(\mathbf{k}^2) \quad (1)$$

with $k_{\pm} = k_x \pm ik_y$, $\epsilon_0(\mathbf{k}) = C + D_1 k_z^2 + D_2 k_{\perp}^2$ and $\mathcal{M}(\mathbf{k}) = M - B_1 k_z^2 - B_2 k_{\perp}^2$. By fitting the energy spectrum of the effective Hamiltonian with that of the *ab initio* calculation, the parameters in the effective model can be determined. For Bi_2Se_3 , our fitting leads to $M = 0.28 \text{ eV}$, $A_1 = 2.2 \text{ eV \AA}$, $A_2 = 4.1 \text{ eV \AA}$, $B_1 = 10 \text{ eV \AA}^2$, $B_2 = 56.6 \text{ eV \AA}^2$, $C = -0.0068 \text{ eV}$, $D_1 = 1.3 \text{ eV \AA}^2$, $D_2 = 19.6 \text{ eV \AA}^2$. Except for the identity term $\epsilon_0(\mathbf{k})$, the Hamiltonian (1) is nothing but the 3D Dirac model with uniaxial anisotropy along the z -direction and \mathbf{k} -dependent mass terms. From the fact

$M, B_1, B_2 > 0$, we can see that the order of the bands $|T_1^+, \uparrow(\downarrow)\rangle$ and $|T_2^-, \uparrow(\downarrow)\rangle$ is inverted around $\mathbf{k} = 0$ compared with large \mathbf{k} , which correctly characterizes the topologically non-trivial nature of the system. Such an effective Dirac model can be used for further theoretical study of the Bi_2Se_3 system, as long as the low-energy properties are considered. For example, as one of the most important low-energy properties of the topological insulators, the topological surface states can be obtained from diagonalizing the effective Hamiltonian equation (1) with an open boundary condition, with the same method used in the study of the 2D quantum spin Hall insulator²⁶. For a surface perpendicular to the z -direction (that is, the $[111]$ direction), k_x, k_y are still good quantum numbers but k_z is not. By substituting $-i\partial_z$ for k_z in equation (1), one can write down the 1D Schrödinger equations for the wavefunctions $\psi_{k_x, k_y}(z)$. For $k_x = k_y = 0$, there are two renormalizable surface-state solutions on the half infinite space $z > 0$, denoted by $|\psi_{0\uparrow}\rangle, |\psi_{0\downarrow}\rangle$. By projecting the bulk Hamiltonian (1) onto the subspace of these two surface states, to the leading order of k_x, k_y , we obtain the following surface Hamiltonian

$$H_{\text{surf}}(k_x, k_y) = \begin{pmatrix} 0 & A_2 k_- \\ A_2 k_+ & 0 \end{pmatrix} \quad (2)$$

in the basis of $|\psi_{0\uparrow}\rangle, |\psi_{0\downarrow}\rangle$. Here, the surface-state wavefunction $|\psi_{0\uparrow(\downarrow)}\rangle$ is a superposition of the $|P_1^+, \uparrow(\downarrow)\rangle$ and $|P_2^+, \uparrow(\downarrow)\rangle$ states, respectively. For $A_2 = 4.1 \text{ eV \AA}$ obtained from the fitting, the Fermi velocity of the surface states is given by $v_F = A_2/\hbar \simeq 6.2 \times 10^5 \text{ m s}^{-1}$, which agrees reasonably well with the *ab initio* results shown in Fig. 4c. In summary, the effective model of the surface states equation (2) characterizes the key features of the topological surface states, and can be used in the future to study the surface-state properties of the Bi_2Se_3 family of topological insulators.

The topological surface states can be directly verified by various experimental techniques, such as ARPES and scanning tunnelling microscopy. In recent years, evidence of surface states has been observed for Bi_2Se_3 and Bi_2Te_3 in ARPES (ref. 27) and scanning tunnelling microscopy²⁸ experiments. In particular, the surface states of Bi_2Te_3 observed in ref. 27 had a similar dispersion to what we obtained in Fig. 4d, which were also shown to be quite stable and robust, regardless of photon exposure and temperature. Near the completion of this work, we became aware of the ARPES experiment²⁹ on Bi_2Se_3 , which measures a Dirac cone near the Γ point of the surface Brillouin zone. These experimental results support the main conclusion of our theoretical work. Moreover, the 3D topological insulators are predicted to exhibit the universal topological magneto-electric effect¹⁰ when the surface is coated with a thin magnetic film. Compared with the $\text{Bi}_{1-x}\text{Sb}_x$ alloy, the surface states of the Bi_2Se_3 family of topological insulators contain only a single Fermi pocket, making it easier to open up a gap on the surface by magnetization and to observe the topological Faraday/Kerr rotation¹⁰ and image magnetic monopole effect³⁰. If observed, such effects would be an unambiguous experimental signature of the non-trivial topology of the electronic properties.

Received 8 December 2008; accepted 1 April 2009;
published online 10 May 2009

References

- Kane, C. L. & Mele, E. J. Quantum spin hall effect in graphene. *Phys. Rev. Lett.* **95**, 226801 (2005).
- Bernevig, B. A. & Zhang, S. C. Quantum spin hall effect. *Phys. Rev. Lett.* **96**, 106802 (2006).
- Kane, C. L. & Mele, E. J. Z_2 topological order and the quantum spin hall effect. *Phys. Rev. Lett.* **95**, 146802 (2005).
- Murakami, S. Quantum spin hall effect and enhanced magnetic response by spin-orbit coupling. *Phys. Rev. Lett.* **97**, 236805 (2006).
- Bernevig, B. A., Hughes, T. L. & Zhang, S. C. Quantum spin hall effect and topological phase transition in HgTe quantum wells. *Science* **314**, 1757–1761 (2006).
- König, M. *et al.* Quantum spin hall insulator state in HgTe quantum wells. *Science* **318**, 766–770 (2007).
- Fu, L., Kane, C. L. & Mele, E. J. Topological insulators in three dimensions. *Phys. Rev. Lett.* **98**, 106803 (2007).
- Moore, J. E. & Balents, L. Topological invariants of time-reversal-invariant band structures. *Phys. Rev. B* **75**, 121306 (2007).
- Roy, R. On the Z_2 classification of quantum spin hall models. Preprint at <<http://arxiv.org/abs/cond-mat/0604211>> (2006).
- Qi, X.-L., Hughes, T. L. & Zhang, S.-C. Topological field theory of time-reversal invariant insulators. *Phys. Rev. B* **78**, 195424 (2008).
- Dai, X., Hughes, T. L., Qi, X.-L., Fang, Z. & Zhang, S.-C. Helical edge and surface states in HgTe quantum wells and bulk insulators. *Phys. Rev. B* **77**, 125319 (2008).
- Hsieh, D. *et al.* A topological dirac insulator in a quantum spin hall phase. *Nature* **452**, 970–974 (2008).
- Fu, L. & Kane, C. L. Topological insulators with inversion symmetry. *Phys. Rev. B* **76**, 045302 (2007).
- Perdew, J. P., Burke, K. & Ernzerhof, M. Generalized gradient approximation made simple. *Phys. Rev. Lett.* **77**, 3865–3868 (1996).
- Fang, Z. & Terakura, K. Structural distortion and magnetism in transition metal oxides: Crucial roles of orbital degrees of freedom. *J. Phys. Condens. Matter* **14**, 3001–3014 (2002).
- Mishra, S. K., Satpathy, S. & Jepsen, O. Electronic structure and thermoelectric properties of bismuth telluride and bismuth selenide. *J. Phys. Condens. Matter* **9**, 461–470 (1997).
- Larson, P. Effects of uniaxial and hydrostatic pressure on the valence band maximum in Sb_2Te_3 : An electronic structure study. *Phys. Rev. B* **74**, 205113 (2006).
- Black, J., Conwell, E. M., Seigle, L. & Spencer, C. W. Electrical and optical properties of some M2-N3-semiconductors. *J. Phys. Chem. Solids* **2**, 240–251 (1957).
- Mooser, E. & Pearson, W. B. New semiconducting compounds. *Phys. Rev.* **101**, 492–493 (1956).
- Wittel, K. & Manne, R. Atomic spin-orbit interaction parameters from spectral data for 19 elements. *Theor. Chim. Acta* **33**, 347–349 (1974).
- Marzari, N. & Vanderbilt, D. Maximally localized generalized wannier functions for composite energy bands. *Phys. Rev. B* **56**, 12847–12865 (1997).
- Souza, I., Marzari, N. & Vanderbilt, D. Maximally localized wannier functions for entangled energy bands. *Phys. Rev. B* **65**, 035109 (2001).
- Sancho, M. P. L., Sancho, J. M. L. & Rubio, J. Quick iterative scheme for the calculation of transfer matrices: Application to Mo (100). *J. Phys. F* **14**, 1205–1215 (1984).
- Sancho, M. P. L., Sancho, J. M. L., Sancho, J. M. L. & Rubio, J. Highly convergent schemes for the calculation of bulk and surface green functions. *J. Phys. F* **15**, 851–858 (1985).
- Winkler, R. *Spin-Orbit Coupling Effects in Two-Dimensional Electron and Hole Systems* (Springer Tracts in Modern Physics, Vol. 191, Springer, 2003).
- Koenig, M. *et al.* The quantum spin hall effect: Theory and experiment. *J. Phys. Soc. Japan* **77**, 031007 (2008).
- Noh, H.-J. *et al.* Spin-orbit interaction effect in the electronic structure of Bi_2Te_3 observed by angle-resolved photoemission spectroscopy. *Europhys. Lett.* **81**, 57006 (2008).
- Urazhdin, S. *et al.* Surface effects in layered semiconductors Bi_2Se_3 and Bi_2Te_3 . *Phys. Rev. B* **69**, 085313 (2004).
- Xia, Y. *et al.* Electrons on the surface of Bi_2Se_3 form a topologically-ordered two dimensional gas with a non-trivial berry's phase. Preprint at <<http://arxiv.org/abs/0812.2078>> (2008).
- Qi, X.-L., Li, R.-D., Zang, J. & Zhang, S.-C. Inducing a magnetic monopole with topological surface states. *Science* **323**, 1184–1187 (2009).

Acknowledgements

We would like to thank B. F. Zhu for the helpful discussion. This work is supported by the NSF of China, the National Basic Research Program of China (No. 2007CB925000), the International Science and Technology Cooperation Program of China (No. 2008DFB00170) and by the US Department of Energy, Office of Basic Energy Sciences under contract DE-AC02-76SF00515.

Additional information

Reprints and permissions information is available online at <http://npg.nature.com/reprintsandpermissions>. Correspondence and requests for materials should be addressed to S.-C.Z.